Research article

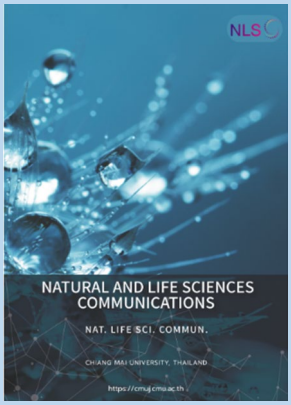

Editor:
Wipawadee Yooin
Chiang Mai University, Thailand

Article history:
Received: May 20, 2023;
Revised: August 31, 2023;
Accepted: September 8, 2023;
Online First: September 12, 2023
https://doi.org/10.12982/NLSC.2023.065

Corresponding author:
Praneet Opanasopit
E-mail: opanasopit_p@su.ac.th

Gold Nanoparticles for Enhanced Skin Permeation of a Protein Drug

Kanokwan Singpanna, Chaiyakarn Pornpitchanarong, Prasopchai Patrojanasophon, Theerasak Rojanarata, Tanasait Ngawhirunpat, Boonnada Pamornpathomkul, and Praneet Opanasopit*

Pharmaceutical Development of Green Innovations Group (PDGIG), Faculty of Pharmacy, Silpakorn University, Nakhon Pathom 73000, Thailand.

ABSTRACT

This study aimed to evaluate the effect of gold nanoparticles (AuNPs) stabilized by citrate ions (Ci-AuNPs) and chitosan (CS-AuNPs) on skin permeation of a protein drug, albumin-fluorescein isothiocyanate conjugate (FITC-BSA). Ci-AuNPs and CS-AuNPs were prepared by the Turkevich method and microwave-assisted method, respectively. The particle size, surface charge, and morphology of the AuNPs were investigated. The skin permeation study through the porcine skin, skin permeation pathway, and the safety of the AuNPs were examined using vertical Franz diffusion cells, confocal laser scanning microscopy (CLSM), and MTT assay, respectively. AuNPs had a spherical shape with size ranging in a nano-scale (<100 nm). Ci-AuNPs exhibited negatively charged surfaces, while CS-AuNPs were positive. A co-delivery of FITC-BSA with CS-AuNPs showed approximately 3.5-fold greater permeability than the FITC-BSA alone. Interestingly, no significant improvement was observed from Ci-AuNPs co-delivery. The CLSM visualization suggested that the delivery of the model protein was enhanced through the transepidermal pathway. Furthermore, the CS-AuNPs presented no significant cytotoxicity toward normal human fibroblasts. Above all, the developed CS-AuNPs were proposed to be safe and effective nanosystem as a skin permeation enhancer for the transdermal delivery of proteins.

Keywords: Gold nanoparticles, Chitosan, Skin permeation enhancer, Protein, Transdermal delivery

Funding: This research was supported by the National Research Council of Thailand (NRCT): N42A650551 and Research and Creative Fund, Faculty of Pharmacy, Silpakorn University.

Citation: Singpanna, K., Pornpitchanarong, C., Patrojanasophon, P., Rojanarata, T., Ngawhirunpat, T., Pamornpathomkul, B., Opanasopit, P. 2023. Gold nanoparticles for enhanced skin permeation of a protein drug. Natural and Life Sciences Communications. 22(4): e2023065.

INTRODUCTION

Transdermal delivery has several advantages over the oral route. For example, drugs administered via the oral route could be degraded by gastric enzymes and undergo first-pass metabolism. Furthermore, skin is a convenient route for self-drug administration which could increase patient compliance (Alkilani et al., 2015). However, the barrier function of the skin is the main obstacle for transdermal delivery, particularly for drugs that are hydrophilic and have a large molecular weight, such as proteins. The outermost layer of the skin, known as the stratum corneum (SC), provides the natural barrier that protects the body from harsh environments (Jeong et al., 2021). The SC is assembled from corneocytes and the extracellular lipid matrix that are aligned like brick and mortar. Those two components are tightly packed, and the dermal absorption is limited to only specific molecules with favorable properties, e.g., MW <500 Da and log P value of 1-4 (N'Da, 2014; Ellison et al., 2020; Supe and Takudage, 2021). With the aim of overcoming this problem, novel strategies for effective dermal delivery have been developed.

Nanoparticles (NPs) have been employed to improve transdermal delivery. In general, they can be divided into lipid-based NPs, polymeric NPs, and metallic NPs. In the field of nanosystems, gold NPs (AuNPs) have been widely studied in pharmaceutical and biomedical applications since they provide good stability and biocompatibility. AuNPs are defined as nano-size gold particles (1-100 nm) that are dispersed in water, making colloidal gold solutions (Chen et al., 2014; Hu et al., 2020). The surface chemistry of AuNPs can be modified for various purposes, and AuNPs have shown to improve transdermal drug delivery by acting as carriers and permeation enhancers (Milan et al., 2022). Also, their surface can be functionalized with various molecules such as polymers, surfactants, and biomolecules, e.g., polysaccharides (Alba-Molina et al., 2019). Chitosan (CS) is an amino polysaccharide derived from the shells of crabs and shrimps (He et al., 2009; Caramella et al., 2010; Lee et al., 2021). Due to its safety and biocompatibility, CS has been widely studied in medical field such as for the treatment of gingivitis (Li et al., 2022), wound regeneration (Elwakil et al., 2020; Yin et al., 2020), and ocular drug delivery (Khangtragool et al., 2008, 2009). Furthermore, CS has been used as a stabilizing agent in AuNP synthesis, and CS-stabilized AuNPs were widely studied to be used in the biomedical field; thus, only a few studies have focused on their use in transdermal delivery (Katas et al., 2018). A study by Jaber et al. (2021) demonstrated that AuNPs capped with CS could enhance the skin permeability of ibuprofen lysate salt over 7 times compared to drug solution. In the case of protein delivery, CS-reduced AuNPs were previously reported to increase insulin permeation across the nasal mucosa for 3-4 times greater than free insulin (Bhumkar et al., 2007). However, to the best of our knowledge, there has been no insightful investigation on CS-stabilized AuNPs (CS-AuNPs) for transdermal delivery. Hence, the aim of this study was to demonstrate the effect of CS-AuNPs compared to citrate-stabilized AuNPs (Ci-AuNPs) on the skin permeability of a model protein drug, albumin-fluorescein isothiocyanate conjugate (FITC-BSA). The physicochemical characteristics, skin permeation pathway, and cytotoxicity of CS-AuNPs were examined.

MATERIALS AND METHODS

Materials

Gold (III) chloride trihydrate ($HAuCl_4 \cdot 3H_2O$, MW = 393.83), fluorescein isothiocyanate conjugated bovine serum albumin (FITC-BSA, MW of albumin = 66 kDa and MW of FITC = 389.4 Da), sodium citrate, low MW chitosan (MW = 50 -190 kDa, 75-85% degree of deacetylation), and other analytical grade chemicals were bought from Sigma-Aldrich (MA, USA). Normal human fibroblasts (NHF) were purchased from ATCC® (VA, USA). Naturally died neonatal pigs were obtained from Charnchai Farm, Ratchaburi, Thailand. All chemical agents used were analytical grade.

Synthesis of AuNPs

Citrate stabilized-AuNPs (Ci-AuNPs)

Ci-AuNPs were synthesized using the Turkevich method. In brief, 95 mL of 0.25 mM gold (III) chloride solution and 5 mL of 1% wt sodium citrate were prepared independently in separate flasks. Next, the flask containing the $HAuCl_4$ solution was covered with a petri dish and heated until boiled (approximately 100°C), then trisodium citrate solution was added. The mixture solution was constantly heated with mechanical stirring for 2-5 min until the solution changed from light yellow to red ruby color, which indicated the transformation of Au^{3+} to Au^0. The gold colloidal solution was cooled in an ice bath and stored at 4°C until use.

Chitosan stabilized-AuNPs (CS-AuNPs)

The microwave-assisted synthesis was employed to synthesize the CS-stabilized AuNPs (CS-AuNPs). The method was conducted as reported by Thanayutsiri et al. (2020). Briefly, 5 mL of low MW CS solution (0.1%wt in 1% acetic acid) and 0.75 mL of 10 mM $HAuCl_4$ solution were combined in a microwave synthesizer glass tube, and a magnetic stirring bar was added. Then, the tube containing the mixture solution was covered with a lid and irradiated with vigorous stirring for 100 sec at 125°C in a microwave synthesizer (Discover SP, CEM Corporation, USA). The gradual change of color from light yellow to ruby red suggested the reduction of Au^{3+} to Au^0, indicating the formation of CS-AuNPs. The obtained gold colloidal solution was cooled immediately in an ice bath and placed at 4°C until use.

Characterization of AuNPs

The particle size, surface charge, and morphology of the AuNPs were investigated. Hydrodynamic diameter, polydispersity index (PDI), and zeta potential (ZP) were measured by zetasizer (Nano ZS, Malvern, UK). The morphology of the synthesized AuNPs was observed under a transmission electron microscope (TEM) (Philips TECNEI 20, FEI Co., Eindhoven, Netherlands) with a voltage of 100 kV and magnification of 135k. The AuNPs were dropped on a copper grid and dried overnight at room temperature prior to the observation with TEM. All measurements were carried out in triplicate and reported as mean ± SD.

In vitro skin permeability of FITC-BSA

The abdominal area of the obtained dead neonatal pig was dissected and used for the *in vitro* permeation test (IVPT). The subcutaneous fat layer was cut using scissors and a surgical blade. The skin was kept at -20°C and thawed with phosphate-buffered solution (PBS, pH 7.4) at room temperature before use. The experiment was employed using the Vertical Franz diffusion cells.

First, the receptor reservoir was filled with 6 mL of PBS, and the skin was fixed between the receptor and donor compartments with the SC facing upward. The temperature of the receptor fluid was controlled by circulating water through the water jacket connecting to a bath circulator (WiseCircu® WCR-P6, Daihan Scientific Co., Seoul, South Korea) to maintain the skin temperature at 32 ± 1 °C. FITC-BSA in the aqueous solution was used as a control. The donor solutions were prepared by simply mixing FITC-BSA with Ci-AuNPs, CS-AuNPs, or CS solution. The final concentration of FITC-BSA was 1 mg/mL in all groups. Then 1 mL of the donor solution was added to the donor compartment. The fluid in the receptor section (0.5 mL) was collected at designated time intervals (1-24 h) for drug quantification. After each sampling, an equivalent volume of fresh PBS was added back to the receptor reservoir. Each experimental group was performed in triplicate. Cumulative drug permeated through the skin was plotted against time. The transdermal flux at steady state (J) was calculated from the slope of the linear portion of the graph. The enhancement ratio (ER) was calculated using equation 1. AuNPs that provided the greatest ER were selected for further investigations.

$$ER = \frac{J_B}{J_A} \quad (1)$$

Where J_B is the transdermal flux at a steady state of FITC-BSA co-delivered with Ci-AuNPs, CS-AuNPs, or CS solution. J_A is the transdermal flux at a steady state of the control (FITC-BSA alone).

FITC-BSA assay

FITC-BSA was prepared by dissolving in PBS and diluted to different concentrations. Then 100 µL of the FITC-BSA solution was placed in a 96-well plate and assayed using a fluorescence spectrophotometer (VICTOR Nivo™ microplate reader, PerkinElmer, Germany) with the excitation and emission wavelength of 495 and 515 nm, respectively. The concentration of FTIC-BSA was computed using a standard curve in the range of 10-50 µg/mL with $R^2 > 0.999$.

Confocal laser scanning microscopy (CLSM) visualization

The skin permeation characteristics of FITC-BSA were investigated based on its fluorescence property using CLSM (Zeiss LSM 800 Airy scan, Carl Zeiss, Jena, Germany). The whole pig skin that covered both follicular and non-follicular region was treated with FITC-BSA (0.1 %wt) using the Franz diffusion apparatus, and the drug was allowed to penetrate for 2 h. Later, the skin was collected, and the excessed drug was eliminated by washing with PBS and wiping with tissue paper. To investigate with CLSM, the immersion oil was dropped on the glass slide, where the collected skin was mounted with the SC facing toward the objective lens. The images of each skin layer were captured in an x-y plane along with the z-axis. ZEN 2 (Blue edition) software was used to render the 3D images.

Cytotoxicity of AuNPs

The cytotoxicity towards NHF of the selected AuNPs was performed by MTT assay. Firstly, the cells were grown in a 96-well plate and seeded to a density of 10,000 cells/well and incubated under a 5% CO_2 atmosphere for 24 h. Next, the cells were incubated with 100 µL of AuNPs (5-75 µg/mL) for 24 h. After that, the cell viability was assessed by replacing the medium with MTT solution (0.5 mg/mL in the medium) and further incubated for 3 h. Finally, the MTT solution was removed and replaced with 100 µL of DMSO. The absorbance was

measured at 550 nm using a microplate reader (VICTOR Nivo™ microplate reader, PerkinElmer, Germany). The percentage of cell viability was calculated using equation 2, and the untreated cell was used as a control.

$$\% \text{ Cell viability} = \frac{Abs_{AuNPs}}{Abs_{control}} \times 100 \qquad (2)$$

Statistical analysis

Each experiment was carried out in triplicate, and the results were reported as mean ± S.D. The data analysis was employed using analysis of variance (ANOVA), followed by followed by Tukey's test for post-hoc analysis. Statistical difference was indicated when $P < 0.05$.

RESULTS

Characterization of AuNPs

Ci-AuNPs and CS-AuNPs used in the present study were synthesized based on a chemical reduction approach. The Au^{3+} ion was reduced to Au^{0} by the reducing agents and stabilized by the stabilizing agents. Citrate ions and CS acted as reducing and stabilizing agents for Ci-AuNPs and CS-AuNPs, respectively. The resulting AuNPs appeared in ruby red color. The hydrodynamic diameter of AuNPs was determined by measuring their particle size using dynamic light scattering (DLS). The polydispersity index (PDI) was also measured to indicate the size distribution. Furthermore, the zeta potential (ZP) value was determined using a Zetasizer to measure the surface charge of both Ci-AuNPs and CS-AuNPs. The hydrodynamic diameter, PDI, and ZP of AuNPs were presented in Table 1.

Table 1. Hydrodynamic diameter, PDI, and ZP of Ci-AuNPs and CS-AuNPs.

Formulations	Hydrodynamic diameter (nm)	PDI	ZP (mV)
Ci-AuNPs	36.51 ± 1.67	0.50 ± 0.01	-30.27 ± 1.37
CS-AuNPs	41.08 ± 0.88	0.28 ± 0.01	+30.97 ± 1.29

The morphology of the AuNPs observed under TEM is presented in Figure 1. The synthesized AuNPs are spherical, and the particles were confirmed to be within the nano-scale with no aggregation found.

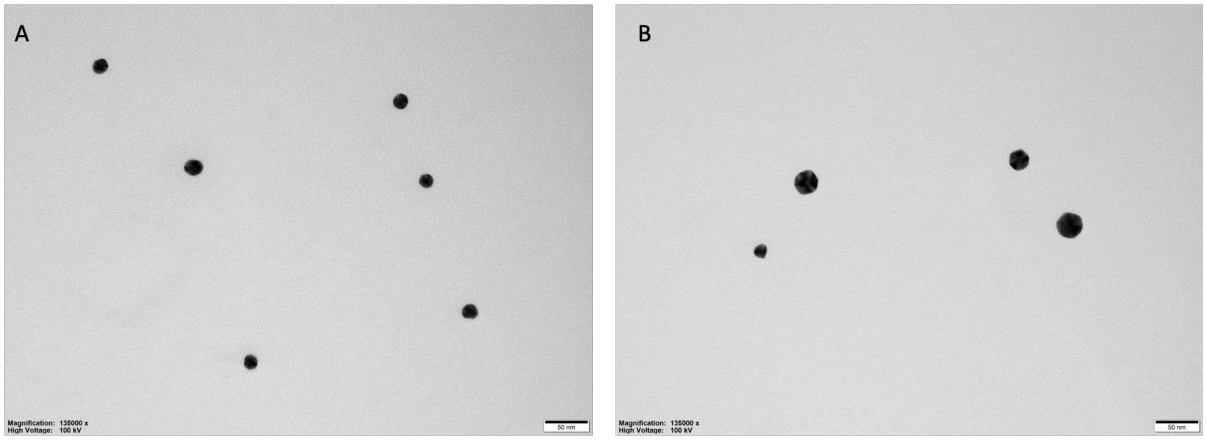

Figure 1. TEM images of (A) Ci-AuNPs and (B) CS-AuNPs at 135k × magnification.

In vitro skin permeability study

The skin permeation profile and the enhancement ratio (ER) of FITC-BSA were presented in Figure 2 and Figure 3, respectively. The results revealed that CS-AuNPs could improve the permeability of FITC-BSA through the pig skin with the ER of 3.51 ± 1.27, and no enhancement effect was noticed from the Ci-AuNPs or the CS solution. Furthermore, it was confirmed that the particle size and zeta potential of both Ci-AuNPs and CS-AuNPs remained unchanged during the skin permeation experiment at 32°C, indicating their stability throughout the duration of the experiment.

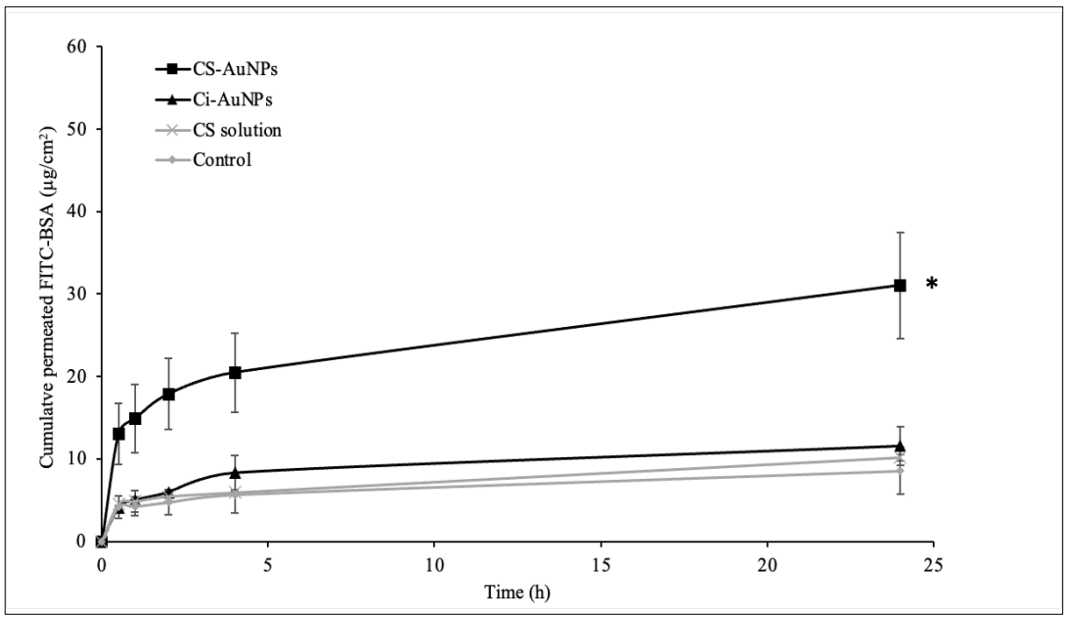

Figure 2. The skin permeation profiles of FITC-BSA co-delivered with CS-AuNPs, Ci-AuNPs, and CS solution. FITC-BSA in an aqueous solution was used as a control. Each data point represents the mean ± SD (n=3). *P<0.05 vs control.

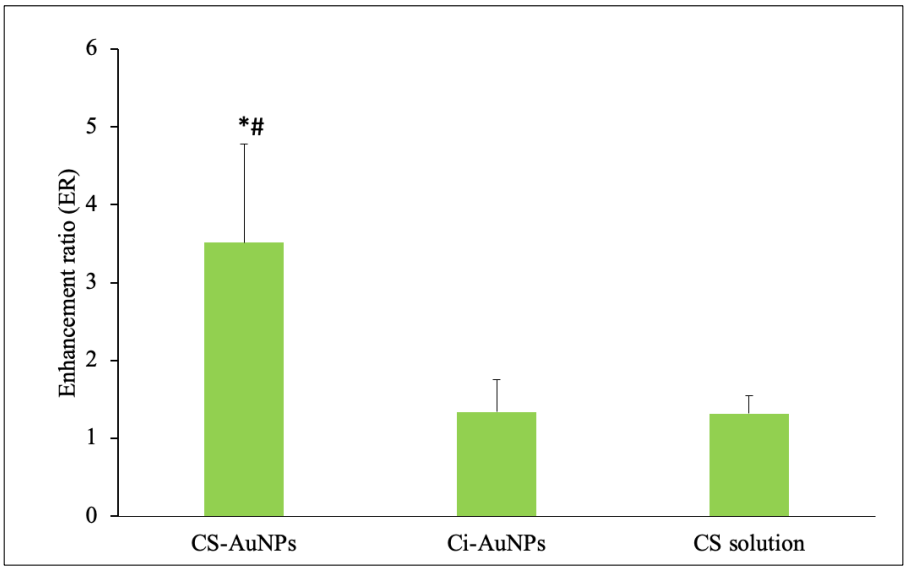

Figure 3. The enhancement ratios of FITC-BSA co-delivered with CS-AuNPs, Ci-AuNPs, and CS solution. Each value represents the mean ± SD (n=3). *P<0.05 vs Ci-AuNPs, #P<0.05 vs CS solution.

CLSM visualization of skin permeation

According to the result of skin permeation study, it was found that only CS-AuNPs had the ability to enhance the skin permeation of FITC-BSA. Therefore, they were chosen for further investigation in the CLSM study. In this CLSM study, the effect of CS-AuNPs on FITC-BSA permeation behavior was investigated. FITC-BSA was seen as a green fluorescence under CLSM. The follicular and non-follicular segments were the regions of interest observed. The three-dimensional CLSM images of FITC-BSA permeation when co-delivered with CS-AuNPs and FITC-BSA alone (control) were presented in Figure 4. At the non-follicular regions, higher fluorescence intensity was perceived after the co-treatment with CS-AuNPs for 2 h (Figure 4B) compared to the control (Figure 4A). However, no significant difference in skin permeation was observed between the FITC-BSA and CS-AuNPs codelivery with FITC-BSA in the follicular region (data not shown).

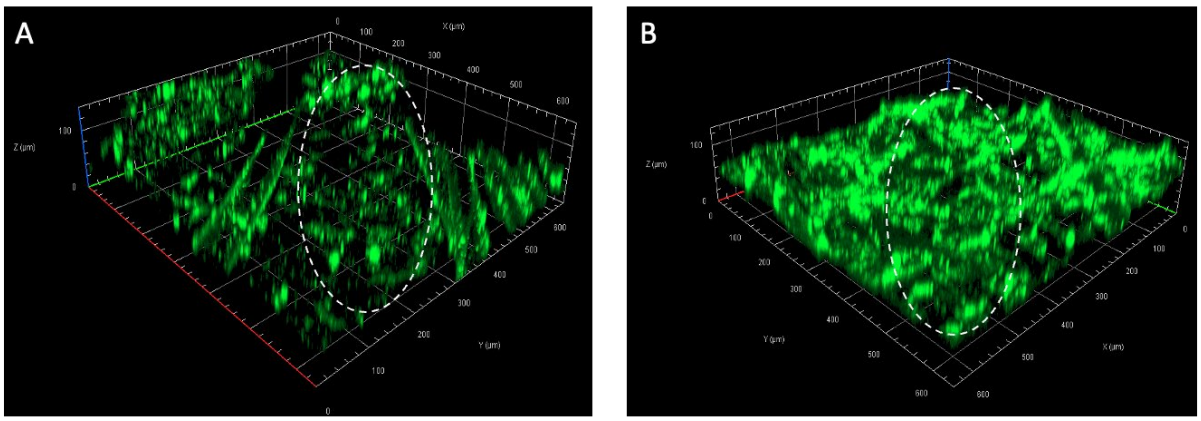

Figure 4. CLSM images of FITC-BSA permeation at non-follicular region (the circled area) of (A) control (B) FITC co-delivered with CS-AuNPs.

Cytotoxicity of CS-AuNPs

The MTT assay was used to evaluate the initial safety of CS-AuNPs toward human skin fibroblasts. From the results in Figure 5, no significant cytotoxicity was noticed after a 24-h period of treatment with the NPs at concentrations ranging from 5 to 75 µg/mL. It was noted from the skin permeability test that the concentration of CS-AuNPs exposed to the skin was 75 µg/mL; hence, this concentration was the highest concentration tested.

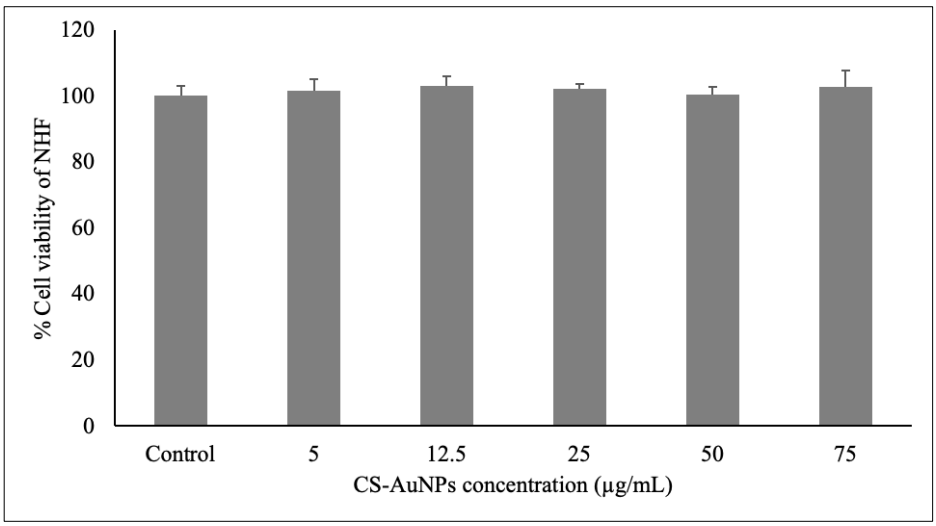

Figure 5. Cell viability of NHF after the treatment with CS-AuNPs for 24 h.

DISCUSSION

The resulting gold colloidal dispersions appeared in ruby red-colored solutions due to the unique property of AuNPs known as surface plasmon resonance (SPR). In short, SPR is a phenomenon that the electrons of Au particles are excited by light which results in the absorption of the green light region and the reflection of the red-light wavelengths (Yeh et al., 2012; El-Sayed et al., 2016; Jeon et al., 2019). The results in Table 1 revealed that both Ci-AuNPs and CS-AuNPs were within a nano-size range (< 100 nm) with narrow size distribution. Considering the ZP of the AuNPs, Ci-AuNPs had a negative ZP of -30 mV because of the citrate ions stabilizing on the surfaces. In contrast, the CS-AuNPs expressed a positive ZP of +30 mV due to the protonated amine functional groups in the CS structure (Thanayutsiri et al., 2020). According to the methods for AuNPs synthesis, the microwave-assisted method has several advantages over the conventional heating method using a hot plate. The conventional heating method has long been known to be inefficiency and time-consuming since the heat is slowly transferred by convection and conduction from the furnace to the reacting system. On the other hand, microwave could generate heat through direct interaction with material, resulting in faster and more energy-efficient reaction (Grewal et al., 2013).

For transdermal drug delivery, AuNPs could act as a permeation enhancer and improve the skin permeation of various molecules, ranging from small drugs to macromolecules. The potential mechanism of AuNPs might be related to the disruption of the lipid matrix and the formation of reversible channels in the SC, thus resulting in the allowance of external molecules to penetrate (Huang et al., 2010; Anirudhan and Nair, 2018). Moreover, the surface modification of AuNPs is considered one of the major keys in skin delivery

(Chen and Feng, 2022). Since Ci-AuNPs have been extensively researched for transdermal delivery and exhibit different physicochemical properties (e.g., surface charge), Ci-AuNPs were chosen as a comparison to CS-AuNPs (Sibuyi et al., 2021). The greater skin permeability provided by CS-AuNPs could be associated with their positive surface charge. As the skin is negatively charged under physiological conditions, the positively charged particles could conveniently interact with the skin via the electrostatic interaction. Also, such interaction could link to the disorder of the tight junction-associated proteins in the SC and result in increased drug permeation (He et al., 2009; Mikusova and Mikus, 2021). According to the results, CS-AuNPs provided the greatest permeability of the model protein, FITC-BSA.

In general, exogenous molecules can penetrate the skin *via* two pathways, the transepidermal and transappendageal routes. The transepidermal route can be subclassified into two paths: transcellular (the permeation across the alternate layers of the lipid matrix and corneocytes) and intercellular pathway (the permeation through the lipid matrix layers between cells). Small lipophilic molecules usually diffuse through intercellular lipid matrix, where most hydrophilic drugs and large permeants are excluded. The transappendageal route included the permeation via hair follicles and sweat ducts, where the hydrophilic and large molecules can enter (Shaker et al., 2019). FITC-BSA is a large hydrophilic permeant that predominantly diffuses via the follicular pathway but not the transepidermal route due to the SC lipid barrier. The CLSM images in Figure 4 suggested that CS-AuNPs could enhance the permeation of the hydrophilic protein *via* the transepidermal route and not the hair follicle route. The exact mechanism of CS-AuNPs is not clearly understood, but the previous reports suggested that AuNPs could alter the lipid organization in SC and thus increase the permeability (Huang et al., 2010; Anirudhan and Nair, 2018). Besides the SC, tight junctions (TJs) are also considered a barrier to transdermal drug delivery. TJ can be found in the epidermis and other epithelia, such as the inner ear membranes (Brandner et al., 2015; Bäsler et al., 2016; Yokouchi and Kubo, 2018). Previous *in vivo* study revealed that CS-AuNPs could impair TJ proteins (occludin and ZO-1 protein) at the inner ear membrane of the mice and enhance the paracellular permeability (Lin et al., 2021). However, the effects of CS-AuNPs on the skin TJs have not yet been reported, and further investigations are needed.

In vitro cytotoxicity of CS-AuNPs was evaluated using MTT assay, and the results could confirm the safety of CS-AuNPs at an initial stage of toxicity evaluation. However, further assessments, such as clinical safety, possible systemic effects, skin irritation, etc., should be investigated further, prior to the application of CS-AuNPs in the pharmaceutical and cosmetic industries.

CONCLUSION

The synthesized Ci-AuNPs and CS-AuNPs were achieved with good size and shape uniformity and had no cytotoxicity to toward human fibroblasts. CS-AuNPs could enhance the skin permeability of a model protein by approximately 3.5 times through the transepidermal pathway, whereas the Ci-AuNPs showed no enhancement effect. These findings suggested that CS-AuNPs were proposed as a promising skin permeation enhancer of protein drugs and macromolecules in pharmaceutical applications. However, further investigations on different aspects, such as pre-clinical and clinical safety should be established.

ACKNOWLEDGMENTS

This research was funded by the National Research Council of Thailand (NRCT): N42A650551 and Research and Creative Fund, Faculty of Pharmacy, Silpakorn University.

AUTHOR CONTRIBUTIONS

Kanokwan Singpanna: Investigation, Formal analysis, Writing - Original. Chaiyakarn Pornpitchanarong and Prasopchai Patrojanasophon: Writing - Review & Editing. Theerasak Rojanarata: Methodology. Tanasait Ngawhirunpat: Conceptualization, Boonnada Pamornpathomkul: Validation, Visualization. Praneet Opanasopit: Visualization, Supervision, Funding acquisition, Project administration. All authors have read and approved the final manuscript.

CONFLICT OF INTEREST

The authors confirm that there is no conflict of interest.

REFERENCES

Alba-Molina, D., Giner-Casares, J.J., Cano, M., 2019. Bioconjugated plasmonic nanoparticles for enhanced skin penetration. Topics in Current Chemistry (Cham). 378: 8.

Alkilani, A.Z., McCrudden, M.T., Donnelly, R.F., 2015. Transdermal drug delivery: Innovative pharmaceutical developments based on disruption of the barrier properties of the stratum corneum. Pharmaceutics. 7: 438-470.

Anirudhan, T.S., Nair, S.S., 2018. Gold nanoparticle and hydrophobic nanodiamond based synergistic system: a way to overcome skin barrier function. Bioconjugate Chemistry. 29: 3262-3272.

Bäsler, K., Bergmann, S., Heisig, M., Naegel, A., Zorn-Kruppa, M., Brandner, J.M., 2016. The role of tight junctions in skin barrier function and dermal absorption. Journal of Controlled Release. 242: 105-118.

Bhumkar, D.R., Joshi, H.M., Sastry, M., Pokharkar, V.B., 2007. Chitosan reduced gold nanoparticles as novel carriers for transmucosal delivery of insulin. Pharmaceutical Research. 24: 1415-1426.

Brandner, J.M., Zorn-Kruppa, M., Yoshida, T., Moll, I., Beck, L.A., De Benedetto, A., 2015. Epidermal tight junctions in health and disease. Tissue Barriers. 3: e974451.

Caramella, C., Ferrari, F., Bonferoni, M.C., Rossi, S., Sandri, G., 2010. Chitosan and its derivatives as drug penetration enhancers. Journal of Drug Delivery Science and Technology. 20: 5-13.

Chen, X., Li, Q.W., Wang, X.M., 2014. Gold nanostructures for bioimaging, drug delivery and therapeutics, In: Baltzer, N., Copponnex, T. (Eds.), Precious Metals for Biomedical Applications. Woodhead Publishing, pp. 163-176.

Chen, Y., Feng, X., 2022. Gold nanoparticles for skin drug delivery. International Journal of Pharmaceutics. 625: 122122.

El-Sayed, N., El-Khourdagui, L., Schneider, M., 2016. Chapter 8 - Insights Into Interactions of Gold Nanoparticles With the Skin and Potential Dermatological Applications. pp. 99-113. In: Hamblin, M.R., Avci, P., Prow, T.W. (eds.), Nanoscience in Dermatology. Academic Press. Boston.

Ellison, C.A., Tankersley, K.O., Obringer, C.M., Carr, G.J., Manwaring, J., Rothe, H., Duplan, H., Genies, C., Gregoire, S., Hewitt, N.J., Jamin, C.J., Klaric, M., Lange, D., Rolaki, A., Schepky, A., 2020. Partition coefficient and diffusion coefficient determinations of 50 compounds in human intact skin, isolated skin layers and isolated stratum corneum lipids. Toxicology In Vitro. 69: 104990.

Elwakil, B.H., Awad, D., Hussein, A.A., Harfoush, R.A., Gohar, Y.M., 2020. Chitosan and liposomes nanoparticles encapsulated cinnamon extract: Antiproteolytic activity and wound healing efficiency of diabetic rats running head: Chitosan vs liposomes nanoparticles as drug delivery carriers. Chiang Mai University Journal of Natural Sciences. 19(3):595-611.

Grewal, A., Kumar, K., Redhu, S., Bhardwaj, S., 2013. Microwave assisted synthesis: A green chemistry approach. International Research Journal of Pharmaceutical and Applied Sciences. 3: 278-285.

He, W., Guo, X., Xiao, L., Feng, M., 2009. Study on the mechanisms of chitosan and its derivatives used as transdermal penetration enhancers. International Journal of Pharmaceutics. 382: 234-243.

Hu, X., Zhang, Y., Ding, T., Liu, J., Zhao, H., 2020. Multifunctional gold nanoparticles: A novel nanomaterial for various medical applications and biological activities. Frontiers in Bioengineering and Biotechnology. 8: 990.

Huang, Y., Yu, F., Park, Y.S., Wang, J., Shin, M.C., Chung, H.S., Yang, V.C., 2010. Co-administration of protein drugs with gold nanoparticles to enable percutaneous delivery. Biomaterials. 31: 9086-9091.

Jaber, N., Al-Akayleh, F., Abdel-Rahem, R.A., Al-Remawi, M., 2021. Characterization *ex vivo* skin permeation and pharmacological studies of ibuprofen lysinate-chitosan-gold nanoparticles. Journal of Drug Delivery Science and Technology. 62: 102399.

Jeon, H.B., Tsalu, P.V., Ha, J.W., 2019. Shape effect on the refractive index sensitivity at localized surface plasmon resonance inflection points of single gold nanocubes with vertices. Scientific Reports. 9: 13635.

Jeong, W.Y., Kwon, M., Choi, H.E., Kim, K.S., 2021. Recent advances in transdermal drug delivery systems: A review. Biomaterials Research. 25: 24.

Katas, H., Moden, N.Z., Lim, C.S., Celesistinus, T., Chan, J.Y., Ganasan, P., Suleman Ismail Abdalla, S., 2018. Biosynthesis and potential applications of silver and gold nanoparticles and their chitosan-based nanocomposites in nanomedicine. Journal of Nanotechnology. 2018: 4290705.

Khangtragool, A., Ausayakhun, S., Leesawat, P., Molley, R., Laokul, C., 2008. Stability of chitosan solutions for potential use in ocular drug delivery. Chiang Mai University Journal of Natural Sciences. 7: 209-217.

Khangtragool, A., Ausayakhun, S., Leesawat, P., Molley, R., Laokul, C., 2009. Evaluation of the use of chitosan in ocular drug delivery of vancomycin. Chiang Mai University Journal of Natural Sciences. 8: 1-9.

Lee, J.S., Oh, H., Kim, S., Lee, J.H., Shin, Y.C., Choi, W.I., 2021. A novel chitosan nanosponge as a vehicle for transepidermal drug delivery. Pharmaceutics. 13(9): 1329.

Li, M., Kamdenlek, P., Kuntanawat, P., Eawsakul, K., Porntaveetus, T., Osathanon, T., Manaspon, C., 2022. *In vitro* preparation and evaluation of chitosan/pluronic F-127 hydrogel as a local delivery of crude extract of Phycocyanin for treating gingivitis. Chiang Mai University Journal of Natural Sciences. 21(4): e2022052.

Lin, Y.C., Shih, C.P., Chen, H.C., Chou, Y.L., Sytwu, H.K., Fang, M.C., Lin, Y.Y., Kuo, C.Y., Su, H.H., Hung, C.L., Chen, H.K., Wang, C.H., 2021. Ultrasound microbubble-facilitated inner ear delivery of gold nanoparticles involves transient disruption of the tight junction barrier in the round window membrane. Frontiers in Pharmacology. 12: 689032.

Mikusova, V., Mikus, P., 2021. Advances in chitosan-based nanoparticles for drug delivery. International Journal of Molecular Sciences. 22(17): 9652.

Milan, J., Niemczyk, K., Kus-Liśkiewicz, M., 2022. Treasure on the earth-gold nanoparticles and their biomedical applications. Materials. 15(9): 3355.

N'Da, D.D., 2014. Prodrug strategies for enhancing the percutaneous absorption of drugs. Molecules. 19: 20780-20807.

Shaker, D.S., Ishak, R.A.H., Ghoneim, A., Elhuoni, M.A., 2019. Nanoemulsion: A review on mechanisms for the transdermal delivery of hydrophobic and hydrophilic drugs. Scientia Pharmaceutica. 87: 17.

Sibuyi, N.R.S., Moabelo, K.L., Fadaka, A.O., Meyer, S., Onani, M.O., Madiehe, A.M., Meyer, M., 2021. Multifunctional gold nanoparticles for improved diagnostic and therapeutic applications: A review. Nanoscale Research Letters. 16: 174.

Supe, S., Takudage, P., 2021. Methods for evaluating penetration of drug into the skin: A review. Skin Research and Technology. 27: 299-308.

Thanayutsiri, T., Patrojanasophon, P., Opanasopit, P., Ngawhirunpat, T., Plianwong, S., Rojanarata, T., 2020. Rapid synthesis of chitosan-capped gold nanoparticles for analytical application and facile recovery of gold from laboratory waste. Carbohydrate Polymers. 250: 116983.

Yeh, Y.C., Creran, B., Rotello, V.M., 2012. Gold nanoparticles: preparation, properties, and applications in bionanotechnology. Nanoscale. 4: 1871-1880.

Yin, H., Udomsom, S., Kantawong, F., 2020. Fabrication of blended gelatin–polyvinyl alcohol-chitosan scaffold for wound regeneration. Chiang Mai University Journal of Natural Sciences. 19: 930-952.

Yokouchi, M., Kubo, A., 2018. Maintenance of tight junction barrier integrity in cell turnover and skin diseases. Experimental Dermatology. 27: 876-883.

OPEN access freely available online
Natural and Life Sciences Communications
Chiang Mai University, Thailand. https://cmuj.cmu.ac.th